Carbohydrate Polymers 105 (2014) 41–48

Contents lists available at ScienceDirect

Carbohydrate Polymers

journal homepage: www.elsevier.com/locate/carbpol

Mechanical properties, biocompatibility, and biodegradation of cross-linked cellulose acetate-reinforced polyester composites

Chin-San Wu*

Department of Chemical and Biochemical Engineering, Kao Yuan University, Kaohsiung County 82101, Taiwan, ROC

ARTICLE INFO

Article history:
Received 25 March 2013
Received in revised form 16 January 2014
Accepted 19 January 2014
Available online 29 January 2014

Keywords:
Poly(hydroxyalkanoate)
Cellulose acetate
Crosslinking technique
Biocompatibility
Biodegradation

ABSTRACT

Composites of treated (cross-linked) cellulose acetate (t-CA) and acrylic acid-grafted poly(hydroxyalkanoate) (PHA-g-AA/t-CA) exhibited noticeably superior mechanical properties compared with PHA/CA composites due to greater compatibility between the two components. The dispersion covering of t-CA in the PHA-g-AA matrix was highly homogeneous as a result of condensation reactions. Human lung fibroblasts (FBs) were seeded on these two series of composites to characterize the biocompatibility properties. In a time-dependent course, the FB proliferation results demonstrated higher performance from the PHA/CA series of composites than from the PHA-g-AA/t-CA composites. The water resistance of PHA-g-AA/t-CA was higher than that of PHA/CA, although the weight loss of both composites buried in *Acetobacter pasteurianus* (*A. pasteurianus*) indicated that they were both biodegradable, especially at higher levels of cellulose acetate substitution. The PHA/CA and PHA-g-AA/t-CA composites were more biodegradable than pure PHA, implying a strong connection between cellulose acetate content and biodegradability.

1. Introduction

Because of waste disposal problems there is increasing interest in the development of biodegradable polymers that can replace traditional plastics. Currently this, polymer research has focused mainly on biodegradable aliphatic plastics and the frequently used biosynthetic aliphatic polymers, including polylactic acid (PLA), polycaprolactone (PCL), and poly(hydroxyalkanoates) (PHA) (Chen et al., 2013; Jazkewitsch, Mondrzyk, Staffel, & Ritter, 2011; Ruth et al., 2007). Hundreds, or even thousands, of years are required to degrade traditional plastic, such as polyphenylene propylene (PP) and polyethylene (PE; Ito & Nagai, 2008; Shih, Huang, & Chen, 2010). In comparison, PHA, developed in recent years, is a biodegradable aliphatic (polyester) plastic that requires only a few months' time to degrade completely into a natural product. Because the majority of the PHA monomer is a copolymer constituted by 3-hydroxy fatty acid with carbon atoms in a chain length of 3–14 and is manufactured from natural renewable resources, it could be completely biodegraded, and possesses excellent plasticity, easy processing and forming characteristics, and biocompatibility (Chanprateep, Buasri, Muangwong, & Utiswannakul, 2010; Ha & Cho, 2002).

Biodegradable plastic prices remain much higher than that of petrochemical material-based plastic products. To lower the cost while considering environmental protection, natural biodegradable polymers, such as natural fiber, are blended into the material (Azwa, Yousif, Manalo, & Karunasena, 2013; Faruk, Bledzki, Fink, & Sain, 2012; Jawaid & Abdul Khalil, 2011). Natural fiber material has many advantages, including low density, low cost, and renewability; however, most importantly, such natural fiber material is biodegradable and nontoxic (Behera, Avancha, Basak, Sen, & Adhikari, 2012; Tian, Tang, Zhuang, Chen, & Jing, 2012). Among such natural fibers, adding wood fiber (lignocellulosic) filler into the thermoplastic has drawn the most attention because plastic can coat a natural fiber during the fiber and plastic mixing process. This significantly reduces the water absorption of the pure wood material and improves the durability of the end product (Frollini, Bartoluccia, Sisti, & Celli, 2013).

Cellulose acetate (CA) is an important and commonly used derivative of natural cellulose fibers (Cheng, Dowd, Selling, & Biswas, 2010; Fan et al., 2013). However, due to the weak binding force between natural fiber and a polyester-based polymer, particularly poor mechanical properties arise when too much natural fiber is added. Many studies have attempted to find a suitable compatibilizing agent or cross-linking agent to improve the interfacial compatibility between the natural fiber and plastic. To increase the adherence between the natural fibers and polyester during processing and mixing, Ibrahima, Dufresne, El-Zawawya, and Agblevorc (2010) used maleic anhydride (MA)-grafted polyester

* Tel.: +886 7 6077685; fax: +886 7 6077788.
E-mail addresses: t50008@cc.kyu.edu.tw, cws1222@cc.kyu.edu.tw

0144-8617/$ – see front matter © 2014 Elsevier Ltd. All rights reserved.
http://dx.doi.org/10.1016/j.carbpol.2014.01.062

plastic as the interface compatibility agent between the polyester plastic and natural fiber, which greatly improved the mechanical strength of the composite material. Fernandes, Correlo, Mano, and Reis (2013) added a coupling agent to the polymer plastic to enhance the reinforcing effect between the polymer plastic and natural fiber. The results showed great improvement in terms of mechanical strength.

In this study, we investigated the mechanical properties, biocompatibility, and biodegradability of CA composites, with PHA and acrylic acid-grafted PHA. The composites were characterized using Fourier-transform infrared spectroscopy (FTIR) and ^{13}C nuclear magnetic resonance (NMR) to identify the bulk structural changes induced by the acrylic acid moiety. Additionally, the effects of CA content on biocompatibility and the cell proliferation rate of human dermal fibroblasts (FBs) on these membranes were evaluated for appropriate properties for wound dressing. Water absorption and the weight loss of blends exposed to *Acetobacter pasteurianus* were also measured as indicators of water resistance and biodegradability.

2. Materials and methods

2.1. Materials

Commercial-grade PHA (EM 5400F) was obtained from Shenzhen Ecomann Biotechnology Co., Ltd. (Shenzhen, China). Acrylic acid (AA), benzoyl peroxide (BPO), and dimethyl sulfoxide (DMSO) were purchased from Sigma-Aldrich Chemical Inc. (St. Louis, MO, USA). 3-(4,5-Dimethylthiazol-2-yl)-2,5-diphenyltetrazoleliumbromide (MTT) was obtained from Promega (Madison, WI, USA). Fetal bovine serum (FBS) and Dulbecco's modified Eagle's medium (DMEM) were purchased from Gibco-BRL (Gaithersburg, MD, USA). Tetraethoxysilane (TEOS) was obtained from Merck KGaA (Frankfurt, Germany). Cellulose acetate (degree of deacetylation: 55%) was supplied by Showa Chemical Co. Ltd. (Tokyo, Japan). All buffers and other reagents were of the highest purity commercially available.

2.2. PHA-g-AA copolymer

The grafting reaction of AA onto PHA is illustrated in Scheme 1A. AA was grafted onto molten PHA in a dichloromethane solution under a nitrogen atmosphere at $30 \pm 1\,^{\circ}C$, and the polymerization reaction was initiated with BPO. The reaction system was stirred at 60 rpm for 6 h. The grafted product (4 g) was then dissolved in 200 mL of refluxing dichloromethane at $30 \pm 1\,^{\circ}C$, and the hot solution was filtered through several layers of cheesecloth. The cheesecloth was washed with acetone to remove the tetrahydrofuran-insoluble unreacted AA, and the product was then dried on the cheesecloth in a vacuum oven at 80 °C for 24 h. The dichloromethane-soluble products in the filtrate were extracted five times using 600 mL of cold acetone for each extraction. The grafting percentage was 6.06 wt% by titration (Wu, 2005). BPO and AA loadings were maintained at 0.3 wt% and 10 wt%, respectively.

2.3. Processing of t-CA

Scheme 1B shows the dissolution of CA in acetone to increase its dispersion in the polymer matrix and to avoid aggregation. The mass ratio of CA to acetone was 1–20. The solution was stirred at room temperature at 50 rpm for 1 h. A mixture of cross-linking agents was prepared by dissolving a stoichiometric amount of TEOS, H_2O, and lactic acid catalyst in tetrahydrofuran, stirring the solution at room temperature for 1 h, and then allowing the solution to stand for 2 days. The molar ratios used were as follows: lactic acid/TEOS = 0.01 and H_2O/TEOS = 2.2. The CA and cross-linking agents were mixed at room temperature for 1 h at a rotor speed of 50 rpm. Samples were prepared with mass ratios of CA to cross-linking agents of 1–5. The final product was dried under vacuum at 105–110 °C for 24 h.

2.4. Composite preparation

Prior to composite fabrication, the CA or t-CA samples were washed with acetone and dried in an oven at 105 °C for 24 h. Composites were prepared in a Brabender (Dayton, OH, USA) "Plastograph" W50EHT 200-Nm mixer with a rotor blade. The blends were mixed at 140–150 °C for 20 min at a rotor speed of 50 rpm. The CA or t-CA contents in the hybrids (PHA/CA or PHA-g-AA/t-CA) were set at 0, 5, 10, 15, and 20 wt%. After mixing, the composites were pressed into thin plates using a hot press and placed in a dryer for cooling. These thin plates were cut into standard sample dimensions for further characterization.

2.5. Characterization

Solid-state ^{13}C NMR spectra were acquired with an AMX-400 NMR spectrometer (Bruker, Billerica, MA, USA) at 100 MHz under cross-polarization, while spinning at the magic angle. Power decoupling conditions were set with a 90° pulse and a 4-s cycle time. Infrared spectra were obtained using an FTS–7PC FTIR spectrophotometer (Bio-Rad, Hercules, CA, USA). The glass-transition temperature (T_g), melting temperature (T_m), and heat of fusion (ΔH_f) were determined with a differential scanning calorimeter (DSC; model 2010; TA Instruments, New Castle, DE, USA). Sample quantities ranged from 4 to 6 mg. Melting curves were recorded between −60 °C and 160 °C at a heating rate of 10 °C min^{-1}. Values of T_g, T_m, and ΔH_f were extracted from the temperatures and areas of the melting peaks in the DSC heating thermograms. A capillary viscometer (Schott AG, Mainz, Germany) was used to measure the intrinsic viscosity of PHA or PHA-g-AA/t-CA dissolved in the dichloromethane solvent at various concentrations (0.5, 1.0, 1.5, and 0.2 g dL^{-1}). The solutions were cleared through a 0.45-μm filter (Lida, Kenosha, WI, USA), and the capillary viscometer was filled with 10 mL of sample and equilibrated in a water bath (B801; Schott AG) at $30.0 \pm 0.1\,^{\circ}C$. Each sample was passed through the capillary tube prior to flow-time measurements. The flow time was used to calculate the relative and reduced viscosities, which were plotted as a function of concentration; the intercept represented the intrinsic viscosity.

2.6. Mechanical testing

A mechanical tester (model LR5K; Lloyd Instruments, Bognor Regis, West Sussex, UK) was used to measure the tensile strength at break, in accordance with ASTM Standard D638. Test samples were prepared in a hydraulic press at 150 °C and conditioned at $50 \pm 5\%$ relative humidity for 24 h before making measurements. Testing was done at a crosshead speed of 20 mm min^{-1}. The mean value was determined from five specimens of each sample.

2.7. Composite morphology

A thin film (150 mm × 150 mm × 1 mm) of each composite was prepared with a hydraulic press and treated with hot water at 60 °C for 24 h. Specimens were cut according to ASTM Standard D638. After rupture, a thin section of the fracture plane was removed. The thin sections were then coated with gold, and the fracture surface morphologies were observed using scanning electron microscopy (SEM; model S-1400; Hitachi, Tokyo, Japan).

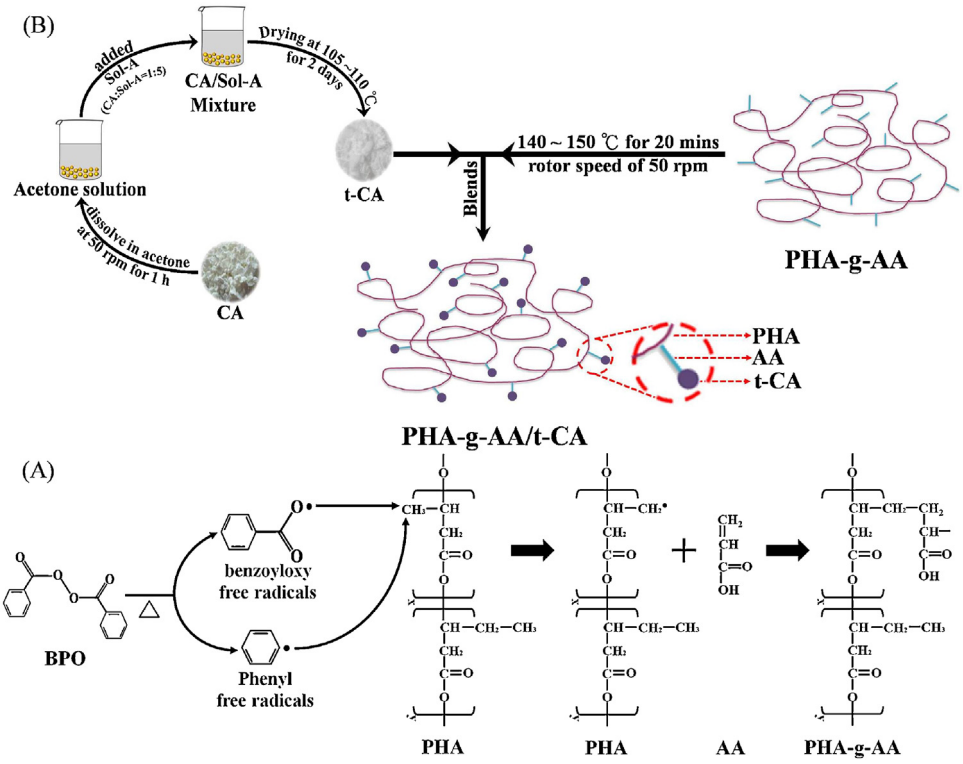

Scheme 1. (A) Grafting reaction of AA onto PHA. (B) Modification of PHA with cross-linked CA and the preparation of composite materials.

2.8. Bio-functions of human lung fibroblasts on the PHA series composites

2.8.1. Cell and culture medium

Human lung FBs (MRC-5) were supplied by the Bioresource Collection and Research Center in Taiwan. The MRC-5 cells were grown in a culture medium [90% Eagle's minimum essential medium (EMEM) with 2 mM L-glutamine and Earle's balanced salt solution (EBSS) adjusted to contain 1.5 g L^{-1} sodium bicarbonate, 0.1 mM nonessential amino acids, and 1.0 mM sodium pyruvate + 10% FBS]. The cells were cultivated at 37 °C in a humidified incubator with a 5% CO_2 atmosphere.

2.8.2. Cell viability assay

The MTT assay was used to evaluate the cytotoxicities of human lung FB cells on the membranes. The sample sheets were contained in 24-well plates and sterilized by ultraviolet light for 1 h. Each well plate was embedded with 5×10^4 human lung FBs, which were incubated with 5% CO_2 at 37 °C for 1, 4, and 7 days. At the end of the incubation period, the media in the plates was discarded, and the cells were washed once with phosphate-buffered saline (PBS). Each well plate was then filled with 100 μL of MTT in a dark environment. The culture was incubated for 4 h to convert the MTT to formazan. The supernatant was then removed, and 150 μL of the DMSO solution was added to dissolve the formazan. The plates were shaken and stirred to ensure the formation of a uniform solution, and the optical density (OD) was read at 540 nm.

2.8.3. Collagen quantification

The composite material sheets were contained in 24-well plates and sterilized by ultraviolet light for 1 h. The well plates were then embedded with 3×10^4 to 6×10^4 human lung FB cells, which were incubated with 5% CO_2 at 37 °C for 24 h. In total, 0.1 mL of the culture fluid from the samples and 1 mL of Sircol dye reagent were mixed in a centrifuge tube for 1 h. The mixed liquid was centrifuged under 12,000 × *g* for 10 min. The supernatant was then removed, and the residual liquid on the edge of the centrifuge tube was removed using absorbent paper. It was necessary to avoid touching the precipitate during the process. Next, 1 mL of an alkali reagent was added to dissolve the precipitate. After 10 min of stable coloration, 0.2 mL was extracted to 96-well plates. The stain was placed into the 96-well plates, and the absorbance was read at 540 nm using a spectrometer plate reader.

2.9. Water absorption

Samples were prepared for water absorption measurements by cutting them into 50 × 30-mm strips (150 ± 5 μm thickness) in accordance with ASTM Standard D570. The samples were dried in a vacuum oven at 50 ± 2 °C for 8 h, cooled in a desiccator, and then immediately weighed to the nearest 0.001 g (this weight was designated W_c). Thereafter, the samples were immersed in distilled water and maintained at 30 ± 2 °C for 120 days. During that time, they were removed from the water at 20-day intervals, gently blotted with tissue paper to remove excess water from their surfaces, immediately weighed to the nearest 0.001 g (this weight was designated W_w), and returned to the water. Each W_w was an average value obtained from three measurements. The percent weight increase due to water absorption (W_f) was calculated to the nearest 0.01%, according to Eq. (1):

$$\%W_f = \frac{W_w - W_c}{W_c} \times 100\%. \quad (1)$$

2.10. Microbiological sample preparation and exposure to A. pasteurianus

A. pasteurianus (BCRC11569) was supplied by the Bioresource Collection and Research Center in Taiwan. The strain was cultivated at 26.0 ± 0.1 °C and stirred at 120 rpm in a medium consisting of 5.0 g yeast extract, 3.0 g peptone, 15.0 g agar, 25.0 g mannitol,

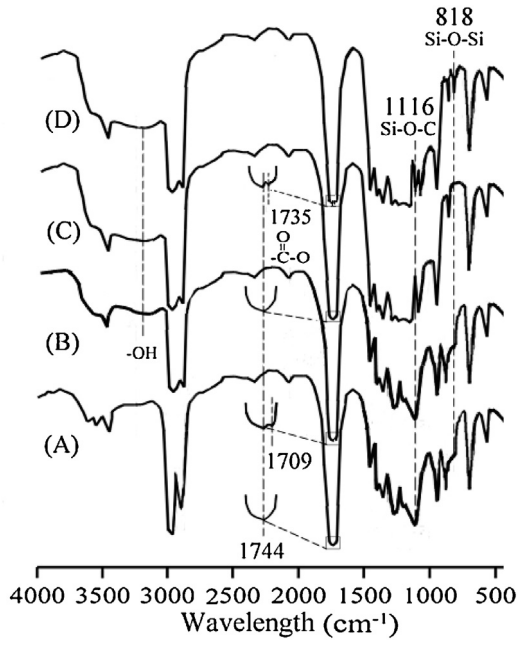

Fig. 1. Fourier-transform infrared spectroscopy (FTIR) spectra of (A) PHA, (B) PHA-g-AA, (C) PHA/CA (10 wt%), and (D) PHA-g-AA/t-CA (10 wt%).

and 1000 mL of distilled water (pH 7.0 ± 0.1). The culture was collected in its early stationary phase for cell entrapment. The samples were then cast into films using a 40 × 15-mm plastic mold. The films were removed from the mold and rinsed several times with distilled water until the waste water had a neutral pH. The films were then clamped to a glass sheet and dried in a vacuum oven (50 ± 2 °C, 0.5 mmHg, 24 h). After drying, the thickness of the films was 0.05 ± 0.02 mm. The dried films were placed in compost Petri dishes, which contained 30 mL of medium and *A. pasteurianus*. These films were then incubated (pH 7.0 ± 0.1; 26.0 ± 0.1 °C; relative humidity: 50 ± 5%). After incubation, the films were washed extensively with deionized water and dried. Each study was conducted using three replicate test reactors and three replicate samples in each test reactor. Each result is therefore based on nine samples.

3. Results and discussion

3.1. Characterization of PHA and its composites

The FTIR spectra of unmodified PHA and PHA-g-AA are shown in Fig. 1A and B, respectively. The characteristic transitions of PHA at 3300–3700, 1700–1760, and 500–1500 cm^{-1} appeared in the spectra of both polymers. Two extra shoulders also appeared in the spectra of the modified PHA: one at 1709 cm^{-1}, which was assigned to —C=O and the free acid in the modified polymer, and the second in the range of 3200–3700 cm^{-1}, which corresponded to a broad O—H stretching transition. This pattern of distinctive peaks indicated successful grafting of AA onto PHA. Similar results have been reported previously (Zhao et al., 2008). Noticeably, changes of peaks at 2800–3000 cm^{-1} were observed as comparing Fig. 1A with other figures in Fig. 1. The changes were due to alteration of C—H in alkane which was caused by grafting AA onto PHA and/or composing CA or t-CA with PHA or AA-g-PHA.

The peak assigned to the O—H stretching vibration from 3200 to 3700 cm^{-1} intensified in the PHA/CA (10 wt%) composite (Fig. 1C) due to contributions from the —OH group of CA. The FTIR spectrum of the PHA-g-AA/t-CA (10 wt%) composite (Fig. 1D) had three peaks at 800–850 cm^{-1}, 1000–1100 cm^{-1}, and 1735 cm^{-1} that were not

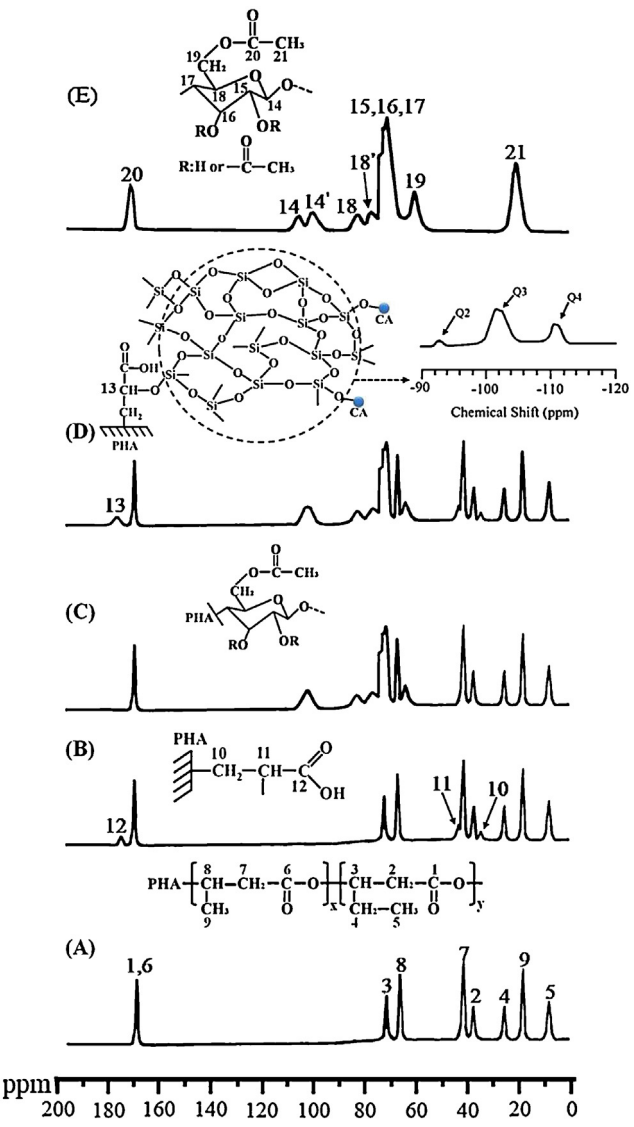

Fig. 2. Solid-state ^{13}C NMR spectra of (A) PHA, (B) PHA-g-AA, (C) PHA/CA (10 wt%), (D) PHA-g-AA/t-CA (10 wt%), and (E) CA.

presented in the FTIR spectrum of the PHA/CA (20 wt%) composite. These peaks were assigned to the asymmetric stretching of Si—O—Si and/or Si—O—C bonds, and the ester carbonyl stretching vibration of the PHA-g-AA/t-CA (10 wt%) composite, respectively (Abdelmouleh, Boufi, Belgacem, & Dufresne, 2007; Huang et al., 2009). These data suggested the formation of branched and cross-linked macromolecules in the PHA-g-AA/t-CA composite by a covalent reaction of the acrylic acid carboxyl groups in PHA-g-AA with the hydroxyl groups of t-CA.

To further confirm this finding, the solid-state ^{13}C NMR spectra of PHA and PHA-g-AA were measured; these spectra are shown in Fig. 2A and B, respectively. Three peaks were observed, corresponding to carbon atoms in the unmodified PHA (1, 6: δ = 169.1 ppm; 2: δ = 38.7 ppm; 3: δ = 71.9 ppm; 4: δ = 26.7 ppm; 5: δ = 9.2 ppm; 7: δ = 40.9 ppm; 8: δ = 67.7 ppm; 9: δ = 19.6 ppm; Keenan, Tanenbaum, Stipanovic, & Nakas, 2004). The ^{13}C NMR spectrum of PHA-g-AA showed additional peaks (10: δ = 36.1 ppm; 11: δ = 42.6 ppm; 12: δ = 174.9 ppm), thereby confirming that AA was covalently grafted onto PHA.

The solid-state ^{13}C NMR spectra of PHA/CA (10 wt%), PHA-g-AA/t-CA (10 wt%), and CA are shown in Fig. 2C–E, respectively.

Relative to unmodified PHA/CA, additional peaks at δ = 36.1 ppm (10) and δ = 42.6 ppm (11) were observed in the spectra of composites containing PHA-g-AA/t-CA. These same features were observed in previous studies (Yu et al., 2007) and indicated grafting of AA onto PHA. However, the peak at δ = 174.9 ppm (C=O; 12; shown in Fig. 2B), which is also typical for AA grafted onto PHA, was absent in the solid-state spectrum of PHA-g-AA/t-CA (10 wt%).

The ^{13}C solid-state NMR and ^{29}Si solid-state NMR spectra of PHA/CA (10 wt%) shown in Fig. 2C also exhibited peaks not observed for neat PHA, which corresponded to the cross-linking agent in the t-CA: Q_2 δ = −91 to −93 ppm, Q_3 δ = −97 to −101 ppm, and Q_4 δ = −110 to −112 ppm (Wu & Liao, 2003). ^{13}C solid-state NMR peaks (13; Fig. 2D), originating from the reaction between AA in PHA-g-AA and —OH in t-CA, were found at δ = 176.8 ppm. These results, combined with the presence of the FTIR peaks at 1735 cm^{-1}, provided further evidence of ester group formation by the condensation of PHA-g-AA with t-CA. The formation of ester groups significantly affected the mechanical and biodegradation properties of PHA-g-AA/t-CA, as discussed in greater detail in the following sections.

3.2. Morphology and mechanical properties of PHA and its composites

In most composite materials, effective wetting and uniform dispersion covering of all components in a given matrix and strong interfacial adhesion between the phases are required to obtain a composite having satisfactory mechanical properties. In the current study, CA or t-CA may be thought of as a dispersed phase within a PHA or PHA-g-AA matrix. SEM was used to evaluate the composite morphology and examine tensile fracture surfaces of PHA/CA (10 wt%) and PHA-g-AA/t-CA (10 wt%) samples. The SEM image of PHA/CA (10 wt%) in Fig. 3A shows that the CA in this composite covered the matrix unevenly. This poor adhesion was due to the formation of hydrogen bonds between the CA, as well as the disparate hydrophilicities of PHA and CA. Poor wetting in these composites was also noted (marked in Fig. 3A) and was attributed to the large difference in surface energies between the CA and PHA matrix (Tran, Fuentes, Dupont-Gillain, Van Vuure, & Verpoest, 2011). The SEM image of PHA-g-AA/t-CA (10 wt%) in Fig. 3B shows more uniform adhesion and better wetting of t-CA in the PHA-g-AA matrix, indicated by the complete coverage of PHA-g-AA on the cellulose acetate, and the removal of both materials when a cellulose acetate was pulled from the bulk. This improved interfacial adhesion was due to the similar hydrophilicity of the two components, which allowed for the formation of branched and cross-linked macromolecules and prevented hydrogen bonding between the t-CA.

Fig. 3C shows the variations in tensile strength at break as a function of CA or t-CA content for the PHA/CA and PHA-g-AA/t-CA composites. The tensile strength at break of pure PHA (16.3 MPa) decreased after grafting with AA (15.9 MPa). The tensile strength at break decreased markedly and continuously with increasing CA content (from 16.3 to 7.8 MPa) for the PHA/CA composites (Fig. 3C). This was attributable to poor dispersion of CA in the PHA matrix, as previously discussed (Fig. 3A). The effect of this incompatibility on the mechanical properties of the composites was substantial. The PHA-g-AA/t-CA composites in Fig. 3C exhibited unique behavior for the tensile strength at break, which increased with increasing t-CA content, despite the fact that PHA-g-AA had a lower tensile strength at break than pure PHA. Furthermore, the tensile strength at break of the PHA-g-AA/t-CA composites was constant or slowly increased with t-CA content greater than 10 wt%. This behavior was likely due to the enhanced dispersion of t-CA in the PHA-g-AA matrix resulting from the formation of branched or cross-linked macromolecules.

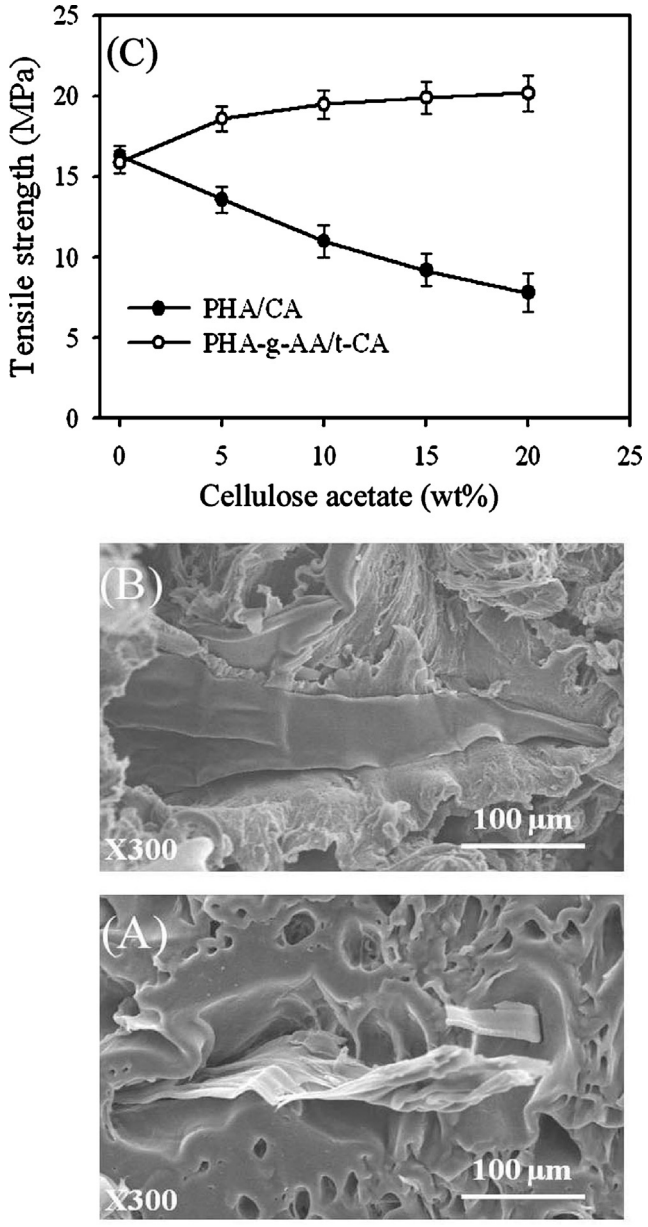

Fig. 3. Scanning electron microscopy (SEM) images of the distribution and adhesion of fibers in (A) PHA/CA (10 wt%) and (B) PHA-g-AA/t-CA (10 wt%) composites. (C) The effect of fiber content on tensile strength at break is shown for PHA/CA and PHA-g-AA/t-CA composites.

3.3. Thermal properties of PHA and its composites

The heats of fusion (ΔH_f), melt temperatures (T_m), and glass transition temperatures (T_g) of PHA/CA and PHA-g-AA/t-CA composites with different cellulose acetate contents were determined using DSC. The results are given in Table 1, which shows that the melting temperature decreased with increasing CA or t-CA content for both PHA/CA and PHA-g-AA/t-CA composites and that the decrease was more noticeable for CA or t-CA content of up to 10 wt%. The lower T_m may have been caused by CA or t-CA lowering the melting viscosity of PHA and PHA-g-AA. The lower melting viscosity of PHA-g-AA/t-CA makes composites easier to process than PHA/CA (Wu & Liao, 2012).

Table 1 also shows that T_g increased with increasing CA or t-CA content for both the PHA/CA and PHA-g-AA/t-CA composites. This increase was likely a result of reduced space available for molecular

Table 1
Influence of cellulose acetate content on the thermal properties of PHA/CA and PHA-g-AA/t-CA composites.

Cellulose acetate (wt%)	PHA/CA			PHA-g-AA/t-CA		
	T_g (°C)	T_m (°C)	ΔH_f (J g^{-1})	T_g (°C)	T_m (°C)	ΔH_f (J g^{-1})
0	−9.6	136.1	41.8	−8.6	135.5	40.3
5	−7.3	134.9	35.8	−3.3	133.9	38.3
10	−6.0	133.9	31.3	+1.0	132.7	36.5
15	−4.9	133.2	28.1	+2.2	132.2	34.6
20	−3.8	132.3	25.2	+3.5	131.8	33.5

motion as the fiber content in the composites increased. T_g values were higher for the PHA-g-AA composite by about 1–5 °C, suggesting that grafting of AA onto the PHA further restricted molecular motion.

The ΔH_f of pure PHA was 41.7 J g^{-1}, whereas that of PHA-g-AA was 40.3 J g^{-1} (Table 1). The lower ΔH_f of PHA-g-AA was attributable to the disruption of regularity in the chain structure and increased spacing between chains due to the grafted branches. The values of ΔH_f in PHA-g-AA/t-CA were approximately 1.5–10.5 J g^{-1} higher than those in PHA/CA. These higher ΔH_f values were attributable to the formation of ester carbonyl groups, as discussed above. ΔH_f may be used as an indicator of blend crystallinity. Although ΔH_f of both the PHA/CA and PHA-g-AA/t-CA blends decreased with increased cellulose acetate content (Table 1), the extent of the decrease was significantly greater in PHA/CA, indicating a lower degree of crystallinity. These results are similar to those obtained elsewhere with composites of polymers and natural fibers (Singh, Mohanty, Sugie, & Takai, 2008). The marked decrease in the crystallinity of such composites was attributable to the hindered motion of the polymer segments due to the presence of natural fiber in the composite matrix (John, Tlili, Anandjiwala, Boudenne, & Ibos, 2012).

3.4. Biocompatibility properties of PHA and its composites

The composites' biocompatibility was evaluated by measuring the cell growth rate of human lung FBs seeded on the membranes (Fig. 4A). The cell viability was examined by MTT assay. The FB cell numbers on different membranes were measured (Fig. 4A). Upon seeding of FBs on the membranes, the PHA/CA series membranes showed similar cell viabilities to FBs seeded on the plate directly from the 1st day to the 7th day, which revealed that the membranes have good compatibility with human lung FBs. With increasing CA or t-CA content, the cell viability did not exhibit obvious differences; at CA or t-CA contents of 5 and 15 wt%, the results were similar (data not shown). The FB cell viabilities on PHA-g-AA membranes were slightly lower than on the plate on the 1st day. However, on the 7th day, the cell viabilities were quite similar to those observed for the PHA/CA series and on the plate.

Sircol dye was used to stain the collagen secreted by human lung FBs on the well and membranes. In Fig. 4B, which compares the seeding of FBs on the plates, the collagen production on different membranes was similar at day 1. At day 4 or 7, collagen production by human lung FBs on PHA/CA was higher than on the plate, the vehicle control. With increasing CA or t-CA content, the collagen production increased. Less collagen was produced in the PHA-g-AA series than in the PHA series; however, this was still more than that produced in the control on day 4. On day 7, the collagen amount produced on the PHA-series membranes increased. These results indicated that PHA-series membranes stimulated collagen secretion in the FBs.

Collagen is an important component for cell proliferation and tissue body formation, which are dependent on FB production (Berglund, Mohseni, Nerem, & Sambanis, 2003). Collagen in an extracellular matrix (ECM) imparts appropriate mechanical strength to the tissue body shape (Naito et al., 2011; Schneider et al., 2010). Therefore, the concentration of collagen secreted is a key indicator of biocompatibility. Because the PHA-series membranes stimulated collagen secretion by FBs, these membranes may be good biomaterials for tissue engineering.

3.5. Water absorption of PHA and its composites

At the same cellulose acetate content, the PHA-g-AA/t-CA composites had a higher resistance to water absorption than the PHA/CA composites (Fig. 5). The water resistance of the PHA-g-AA/t-CA composites was moderate, and the hydrophobicity of t-CA was probably enhanced by interactions with the PHA-g-AA. For both PHA/CA and PHA-g-AA/t-CA, the percent weight gain over the 120-day test period increased as the cellulose acetate content increased.

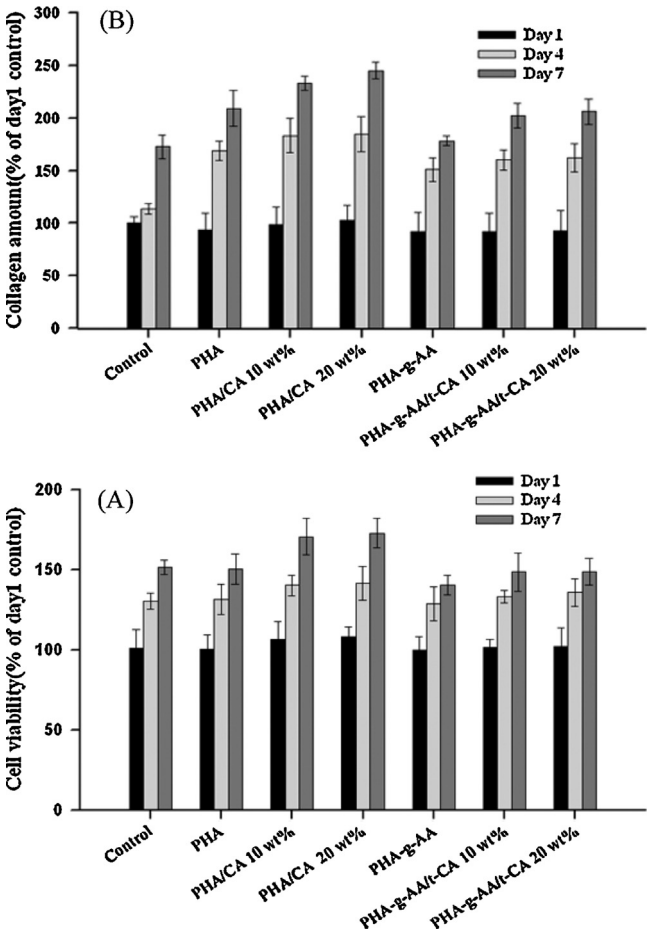

Fig. 4. (A) Cell proliferation ratios of human lung fibroblasts (FBs) seeded on two series membranes. From 1 to 7 days, the cell proliferation rate was quantified by MTT assay. (B) The collagen amount secreted from human lung FBs seeded on two series membranes for 7 days. Sircol dye was used to quantify the collagen amount.

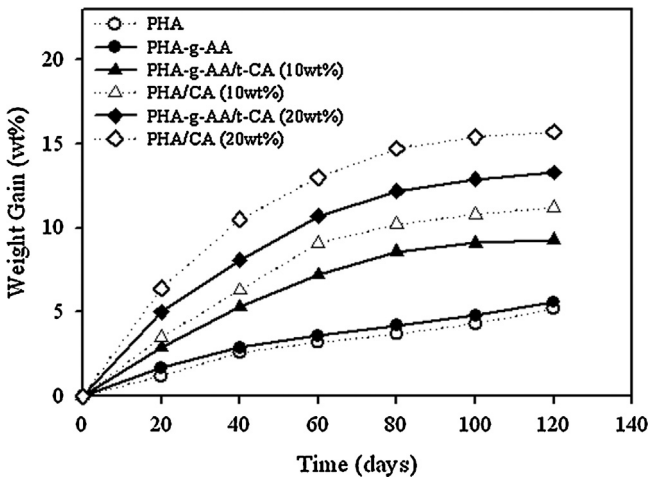

Fig. 5. Percent weight gain from water absorption for PHA/CA and PHA-g-AA/t-CA composites.

Because the arrangement of polymer chains in these systems was supposedly random, the above result was likely due to decreased chain mobility with greater amounts of cellulose acetate, and to the hydrophilic character of the cellulose acetate, which adhered weakly to the more hydrophobic PHA.

3.6. Biodegradation of PHA and its composites

Changes in the morphology of the PHA, PHA/CA, and PHA-g-AA/t-CA composites were noted as a function of the amount of time they were buried in *A. pasteurianus*. SEM images taken after 60 and 120 days illustrated the extent of morphological change (Fig. 6). PHA/CA composites (10 wt%; Fig. 6E and F) exhibited larger and deeper pits that appeared to be more randomly distributed than those in the PHA-g-AA/t-CA (10 wt%) composites (Fig. 6H and I). These analyses also indicated that biodegradation of the CA phase in PHA/CA (10 wt%) increased over time, confirming the results presented in Fig. 6J. After 60 days, the disruption of the PHA matrix became more obvious (Fig. 6B). This degradation was confirmed by the increasing weight loss of the PHA matrix as a function of incubation time (Fig. 6J), which reached nearly 30% after only 120 days. The most likely cause of this weight loss was biodegradation. The SEM images in Fig. 6 indicate that the PHA-g-AA/t-CA (10 wt%) composites were more readily degraded than neat PHA. Moreover, at 60 and 120 days, larger pores were apparent in the PHA-g-AA/t-CA composites (Fig. 6H and I), indicating a higher level of degradation. The rate of weight loss of the PHA-g-AA/t-CA composites also accelerated relative to that of PHA, exceeding 30% after 120 days (Fig. 6J). These results demonstrated that the addition of fiber to the PHA-g-AA enhanced the biodegradability of the composite.

Fig. 6J shows the percent weight change as a function of time for PHA/CA and PHA-g-AA/t-CA composites buried in the *A. pasteurianus*. For both composites, the degree of weight loss increased with

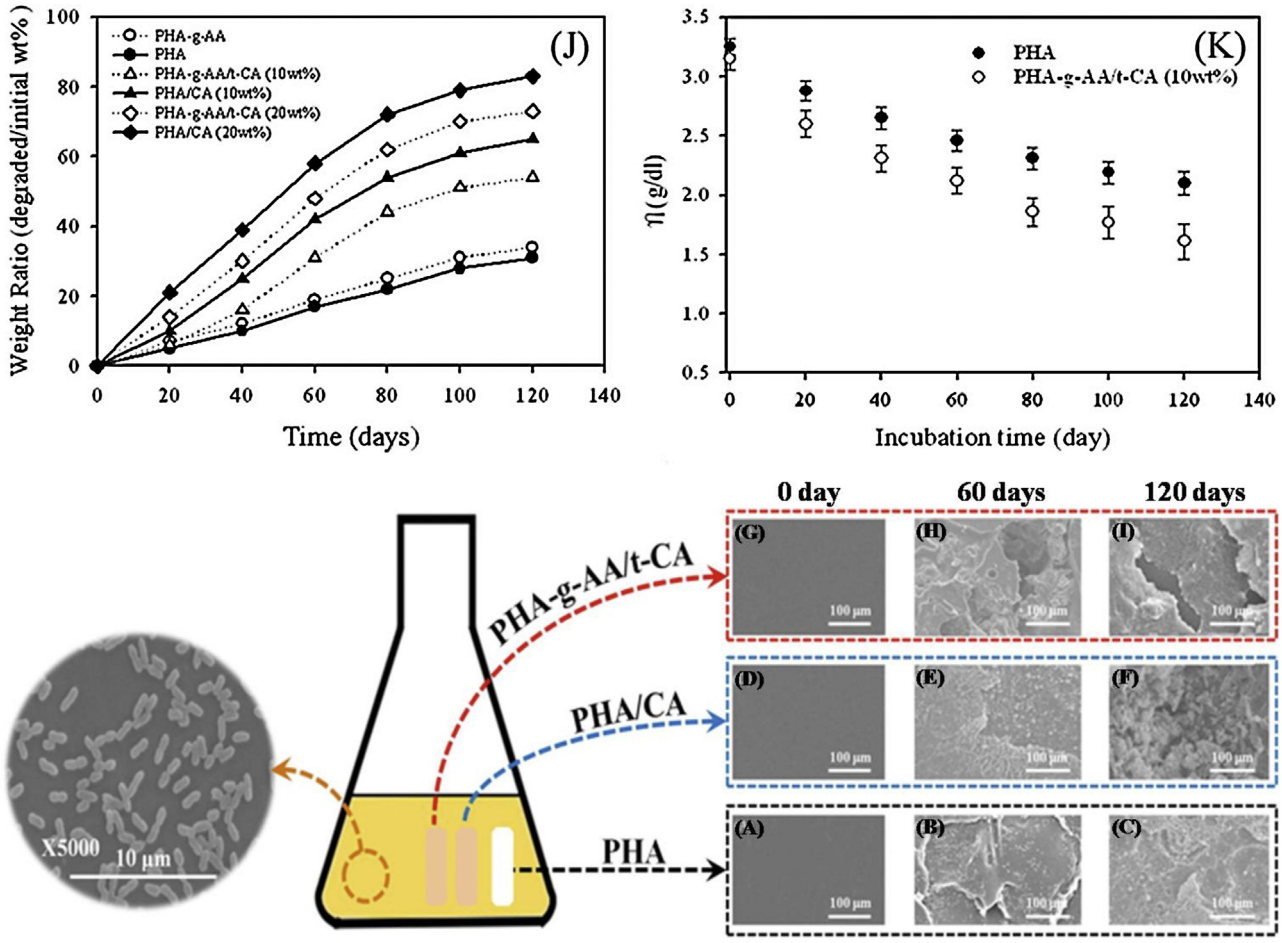

Fig. 6. SEM images showing the morphology of (A–C) PHA, (D–F) PHA/CA (10 wt%), and (G–I) PHA-g-AA/t-CA (10 wt%) films as a function of incubation time in the *Acetobacter pasteurianus* compost. (J) Weight loss percentages of PHA, PHA-g-AA, PHA/CA, and PHA-g-AA/t-CA as a function of incubation time in *A. pasteurianus* compost. (K) Time-course profile of the intrinsic viscosity for PHA and PHA-g-AA/t-CA loaded with *A. pasteurianus*.

cellulose acetate content. Composites with 20 wt% CA degraded rapidly over the first 120 days, losing mass approximately equivalent to their CA content, and they showed a gradual decrease in weight over the next 60 days. PHA/CA exhibited a weight loss of approximately 3–9 wt% more than PHA-g-AA/t-CA.

The change in intrinsic viscosity and molecular weight with incubation time for the PHA and PHA-g-AA/t-CA composites are shown in Fig. 6K. The results show that the intrinsic viscosity for PHA encapsulating *A. pasteurianus* ranged from 2.61 to 1.47 g dL^{-1} over the 0–120-day incubation period, while the values for PHA-g-AA/t-CA were 2.45–0.99 g dL^{-1}. The lower intrinsic viscosity of the latter suggests that a higher number of fragments were present. Another cause of the decreased intrinsic viscosity of PHA-g-AA/t-CA is the conformational changes in the t-CA molecule caused by the formation of an ester functional group.

4. Conclusions

Composites of AA-modified PHA with cross-linked CA were studied. FTIR and NMR analyses revealed the formation of ester groups in the composites formed by reactions between the hydroxyl groups of the t-CA and the acrylic acid carboxyl groups of PHA-g-AA. The morphology of the PHA-g-AA/t-CA composites was consistent, with good adhesion between the t-CA phase and the PHA-g-AA matrix. Mechanical tests showed that the improved adhesion between t-CA and PHA-g-AA enhanced the mechanical properties of the composites, especially the tensile strength. The cell viability tests indicated that PHA membranes have good biocompatibility for FBs to proliferate upon. The collagen secretion by FBs stimulated by PHA series membranes indicated the potential for PHA/CA membranes as biomaterials for tissue engineering. The water resistance of PHA-g-AA/t-CA was higher than that of PHA/CA. When incubated in *A. pasteurianus*, the biodegradation rate of PHA-g-AA/t-CA was lower than that of PHA/CA, but still higher than that of pure PHA. The degree of biodegradation increased with increasing CA content. Overall, the PHA-g-AA/CA composites exhibited good mechanical properties, biocompatibility, and biodegradation. In the future, adjustments to the formula of this composite may be used to optimize its functionality and increase its product utility.

Acknowledgement

The author thanks the National Science Council (Taipei City, Taiwan, ROC) for financial support (NSC-101-2621-M-244-001).

References

Abdelmouleh, M., Boufi, S., Belgacem, M. N., & Dufresne, A. (2007). Short natural-fibre reinforced polyethylene and natural rubber composites: Effect of silane coupling agents and fibres loading. *Composites Science and Technology*, *67*(7–8), 1627–1639.

Azwa, Z. N., Yousif, B. F., Manalo, A. C., & Karunasena, W. (2013). A review on the degradability of polymeric composites based on natural fibres. *Materials & Design*, *47*, 424–442.

Behera, A. K., Avancha, S., Basak, R. K., Sen, R., & Adhikari, B. (2012). Fabrication and characterizations of biodegradable jute reinforced soy based green composites. *Carbohydrate Polymers*, *88*(1), 329–335.

Berglund, J. D., Mohseni, M. M., Nerem, R. M., & Sambanis, A. (2003). A biological hybrid model for collagen-based tissue engineered vascular constructs. *Biomaterials*, *24*(7), 1241–1254.

Chanprateep, S., Buasri, K., Muangwong, A., & Utiswannakul, P. (2010). Biosynthesis and biocompatibility of biodegradable poly(3-hydroxybutyrate-co-4-hydroxybutyrate). *Polymer Degradation and Stability*, *95*(10), 2003–2012.

Chen, W., Zou, Y., Jia, J., Meng, F., Cheng, R., Deng, C., et al. (2013). Functional poly(ε-caprolactone)s via copolymerization of ε-caprolactone and pyridyl disulfide-containing cyclic carbonate: Controlled synthesis and facile access to reduction-sensitive biodegradable graft copolymer micelles. *Macromolecules*, *46*(3), 699–707.

Cheng, H. N., Dowd, M. K., Selling, G. W., & Biswas, A. (2010). Synthesis of cellulose acetate from cotton byproducts. *Carbohydrate Polymers*, *80*(2), 449–452.

Fan, G., Wang, M., Liao, C., Fang, T., Li, J., & Zhou, R. (2013). Isolation of cellulose from rice straw and its conversion into cellulose acetate catalyzed by phosphotungstic acid. *Carbohydrate Polymers*, *94*(1), 71–76.

Faruk, O., Bledzki, A. K., Fink, H.-P., & Sain, M. (2012). Biocomposites reinforced with natural fibres: 2000–2010. *Progress in Polymer Science*, *37*(11), 1552–1596.

Fernandes, E. M., Correlo, V. M., Mano, J. F., & Reis, R. L. (2013). Novel cork–polymer composites reinforced with short natural coconut fibres: Effect of fibre loading and coupling agent addition. *Composites Science and Technology*, *78*, 56–62.

Frollini, E., Bartoluccia, N., Sisti, L., & Celli, A. (2013). Poly(butylene succinate) reinforced with different lignocellulosic fibres. *Industrial Crops and Products*, *45*, 160–169.

Ha, C.-S., & Cho, W.-J. (2002). Miscibility, properties, and biodegradability of microbial polyester containing blends. *Progress in Polymer Science*, *27*(4), 759–809.

Huang, Z., Liang, X., Hu, H., Gao, L., Chen, Y., & Tong, Z. (2009). Influence of mechanical activation on the graft copolymerization of sugarcane bagasse and acrylic acid. *Polymer Degradation and Stability*, *94*(10), 1937–1945.

Ibrahima, M. M., Dufresne, A., El-Zawawya, W. K., & Agblevorc, F. A. (2010). Banana fibres and microfibrils as lignocellulosic reinforcements in polymer composites. *Carbohydrate Polymers*, *81*(4), 811–819.

Ito, M., & Nagai, K. (2008). Degradation issues of polymer materials used in railway field. *Polymer Degradation and Stability*, *93*(10), 1723–1735.

Jawaid, M., & Abdul Khalil, H. P. S. (2011). Cellulosic/synthetic fibre reinforced polymer hybrid composites: A review. *Carbohydrate Polymers*, *86*(1), 1–18.

Jazkewitsch, O., Mondrzyk, A., Staffel, R., & Ritter, H. (2011). Cyclodextrin-modified polyesters from lactones and from bacteria: An approach to new drug carrier systems. *Macromolecules*, *44*(6), 1365–1371.

John, M. J., Tlili, R., Anandjiwala, R. D., Boudenne, A., & Ibos, L. (2012). Effect of amphiphilic coupling agent on heat flow and dielectric properties of flax–polypropylene composites. *Composites: Part B*, *43*(2), 526–532.

Keenan, T. M., Tanenbaum, S. W., Stipanovic, A. J., & Nakas, J. P. (2004). Production and characterization of poly-β-hydroxyalkanoate copolymers from *burkholderia cepacia* utilizing xylose and levulinic acid. *Biotechnology Progress*, *20*(6), 1697–1704.

Naito, Y., Shinoka, T., Duncan, D., Hibino, N., Solomon, D., Cleary, M., et al. (2011). Vascular tissue engineering: Towards the next generation vascular grafts. *Advanced Drug Delivery Reviews*, *63*(4–5), 312–323.

Ruth, K., Grubelnik, A., Hartmann, R., Egli, T., Zinn, M., & Ren, Q. (2007). Efficient production of (R)-3-hydroxycarboxylic acids by biotechnological conversion of polyhydroxyalkanoates and their purification. *Biomacromolecules*, *8*(1), 279–286.

Schneider, R. K., Anraths, J., Kramann, R., Bornemann, J., Bovi, M., Knüchel, R., et al. (2010). The role of biomaterials in the direction of mesenchymal stem cell properties and extracellular matrix remodelling in dermal tissue engineering. *Biomaterials*, *31*(31), 7948–7959.

Shih, Y.-F., Huang, C.-C., & Chen, P.-W. (2010). Biodegradable green composites reinforced by the fibre recycling from disposable chopsticks. *Materials Science and Engineering A*, *527*, 1516–1521.

Singh, S., Mohanty, A. K., Sugie, T., & Takai, Y. (2008). Renewable resource based biocomposites from natural fibre and polyhydroxybutyrate-co-valerate (PHBV) bioplastic. *Composites: Part A*, *39*(5), 875–886.

Tian, H., Tang, Z., Zhuang, X., Chen, X., & Jing, X. (2012). Biodegradable synthetic polymers: Preparation, functionalization and biomedical application. *Progress in Polymer Science*, *37*(2), 237–280.

Tran, L. Q. N., Fuentes, C. A., Dupont-Gillain, C., Van Vuure, A. W., & Verpoest, I. (2011). Wetting analysis and surface characterisation of coir fibres used as reinforcement for composites. *Colloids and Surfaces A*, *377*(1–3), 251–260.

Wu, C. S. (2005). Improving polylactide/starch biocomposite by grafting polylactide with acrylic acid—characterization and biodegradability assessment. *Macromolecular Bioscience*, *5*(4), 352–361.

Wu, C. S., & Liao, H.-T. (2003). Polyethylene-octene elastomer/silica hybrids prepared by the sol–gel process using tetraethoxysilane. *Designed Monomers & Polymers*, *6*(4), 1–13.

Wu, C. S., & Liao, H.-T. (2012). Polycaprolactone-based green renewable ecocomposites made from rice straw fibre: Characterization and assessment of mechanical and thermal properties. *Industrial & Engineering Chemistry Research*, *51*(8), 3329–3337.

Yu, F., Yao, K., Shi, L., Wan, W., Zhong, Q., Fu, Y., et al. (2007). Investigation of acrylic acid polymerization in novel two-dimensional molecular space with regular amino groups of layered aminopropylsilica. *Chemistry of Materials*, *19*(14), 3412–3418.

Zhao, H.-P., Zhu, J.-T., Fu, Z.-Y., Feng, X.-Q., Shao, Y., & Ma, R.-T. (2008). Plasma surface graft of acrylic acid and biodegradation of poly(butylene succinate) films. *Thin Solid Films*, *516*(16), 5659–5663.